

# Modeling the precipitation distribution by radius and pore size during drying of an impregnated sphere

N.V. Peskov

*Faculty of Computational Mathematics and Cybernetics,  
Lomonosov Moscow State University, Moscow, Russian Federation.*

---

## Abstract

The process of preparing heterogeneous catalysts on porous supports includes a drying stage, in which the porous material, impregnated with an aqueous solution of the catalyst precursor, is dried, and the precursor is precipitated on the pore walls. The precipitate distribution throughout the support volume strongly influences the catalyst performance and durability within industrial reactors. This paper presents a mathematical model for simulating the precipitation distribution during the drying of a porous sphere. Examples of calculations are given demonstrating the influence of some parameters on the distribution by space and by pore size.

*Keywords:* catalysts preparation modeling, drying with precipitation model, precipitation distribution in a spherical pellet, numerical solution

---

## 1. Introduction

Heterogeneous catalysts are widely used in the modern chemical industry to accelerate the rate of reactions and change the selectivity of processes in the desired direction. To increase the efficiency of the catalyst, it is advisable to increase the contact area of its active elements with the reagents. This can be done by distributing the active elements over the pore surface in a porous support with a large internal surface area. One of the most common methods for preparing such catalysts is the impregnation method, in which the support is first impregnated with a precursor solution, followed by drying and subsequent calcination [1, 2]. In industrial reactors, such catalysts are

---

*Email address:* peskovnick@gmail.com (N.V. Peskov)

used in the form of millimeter-sized pellets of various shapes, of which the sphere is the most convenient for modeling.

In the models for preparing supported catalysts by impregnation, two mechanisms for placing active elements on pore walls were considered. Chronologically, the first mechanism to be considered was one in which active elements were adsorbed from solution onto the pore walls. In this case, the distribution of active elements in the pore space was mainly formed at the impregnation stage, and subsequent drying only corrected this distribution [3, 4, 5, 6]. This mechanism works in cases where the concentration of the solution is low and the chemical interaction between the solute and solid support is strong enough. In another mechanism, the catalyst precursor in the form of a salt of catalytically active metal is deposited from the super-saturated aqueous solution on the pore walls during the drying step [7, 8].

In this paper, a mathematical model of the second mechanism of placement of the catalyst precursor in the pore space of the support is considered. The model under consideration, like model [7, 8], is based on the Whitaker model of drying porous materials [9, 10] with additional terms describing the precipitation of salt from solution. However, the equation for the gas phase is excluded from the equations of Model [9], since precipitation occurs only in the presence of a liquid solution in the pores. In this case, dynamic equilibrium between the liquid and vapor is usually assumed, i.e., the vapor density is equal to the saturated density. Under these conditions, the equation for the gas phase can be replaced by the requirement that the gas pressure in the pores be equal to the external gas pressure. This substitution has virtually no effect on the overall solution of the model.

The results of calculating the distribution of precipitant along the radius of a sphere in dependence on some model parameters are presented. To simulate precipitant distribution over pores, a capillary bundle model is used, which is used in the Whitaker model to estimate capillary pressure and fluid velocity within pores. It is assumed that sediment settles in those pores (capillaries) that are currently drying.

## 2. Model

A homogeneous porous sphere of radius  $R$  and porosity  $\epsilon = V_p/V$ , where  $V$  is the volume of the sphere and  $V_p$  is the total volume of the pores (voids). The sphere is impregnated with an aqueous solution of a metal salt (we will refer to some properties of ferrous fosphate  $\text{FeSO}_4 \cdot 7(\text{H}_2\text{O})$ ), which serves as

a precursor for the catalyst. It is assumed that the solution does not chemically react with the sphere's material and that the salt concentration in the solution is sufficiently high that salt adsorption on the pore walls can be neglected. After impregnation, the sphere is dried in air at a specified external temperature  $T_{ex}$ , pressure  $P_{g,ex}$ , and humidity  $\varphi_{ex}$  and corresponding water vapor pressure  $P_{v,ex} = \varphi_{ex}P_v^*(T_{ex})$ .  $P_v^*(T)$  is the saturated vapor pressure at temperature  $T$ . During drying, water evaporates from the solution, increasing the salt concentration, and when the solubility threshold is exceeded, the salt precipitates on the pore walls.

### 2.1. Equations

The mathematical description of the drying process of a solution in the pores of a material with precipitation presented here does not take into account mass and heat transfer in the air within the pore space. This is because, according to our computational experience, processes in the gas phase have virtually no effect on the distribution of precipitation. Precipitation occurs during the first stage of drying, when the liquid solution is still present in the pores of the material. The Whitaker drying model typically assumes a dynamic equilibrium between liquid and vapor in the pore space, but the presented model only works in the presence of liquid. Therefore, the equation for the gas phase is omitted, and it is assumed that the water vapor pressure in the pores is equal to the saturated vapor pressure at a given temperature.

The system of equations below describes the evolution of the fraction of the sphere's volume occupied by the solution,  $\epsilon_l(r, t)$ , the mass fraction of the metal salt in the solution,  $\gamma_m(r, t)$  ( $\gamma_w = 1 - \gamma_m$ ), the fraction of the sphere's volume occupied by the precipitate,  $\epsilon_m(r, t)$ , and the temperature  $T(r, t)$  in the radial coordinate  $r$  at time  $t$ . It is assumed that all phases are in thermal equilibrium and the temperature is the same in both the solid and liquid phases.

$$\frac{\partial}{\partial t}(\epsilon_l \rho_l \gamma_w) + \nabla \cdot (\rho_l \gamma_w \mathbf{v}_l) = \nabla \cdot (\epsilon_l \rho_l D_{wm} \nabla \gamma_w), \quad (1)$$

$$\frac{\partial}{\partial t}(\epsilon_l \rho_l \gamma_m) + \nabla \cdot (\rho_l \gamma_m \mathbf{v}_l) = \nabla \cdot (\epsilon_l \rho_l D_{wm} \nabla \gamma_m) - \epsilon_l r_{pr}, \quad (2)$$

$$\frac{\partial}{\partial t}(\epsilon_m \rho_m) = \epsilon_l r_{pr}, \quad (3)$$

$$\frac{\partial}{\partial t}(\epsilon_s \rho_s c_s + \epsilon_l \rho_l c_l + \epsilon_m \rho_m c_m)T + \nabla \cdot (\rho_l c_l T \mathbf{v}_l) = \nabla \cdot (\lambda \nabla T). \quad (4)$$

Equations (1), (2) and (4) are continuity equations for water, dissolved salt, and heat (enthalpy), respectively, taking into account binary diffusion in solution and thermal conductivity. Equation (3) describes the accumulation of precipitated metal salt within the volume of the sphere. The precipitation rate,  $r_{pr}$ , is defined as

$$r_{pr} = k_{pr} \max(0, \gamma_m - \gamma_m^*), \quad (5)$$

where  $k_{pr}$  is the rate constant,  $\gamma_m^*$  is the mass fraction of salt in a saturated solution.

## 2.2. Parameters

Constant parameters of the model:

$\epsilon_s$  is the fraction of the material volume occupied by the solid skeleton,  $\epsilon_s = 1 - \epsilon$ . In this paper,  $\epsilon = 0.6$ , so  $\epsilon_s = 0.4$ .

$\rho$  [kg/m<sup>3</sup>] is the density of substance. Solid skeleton,  $\rho_s = 3000$ ; salt,  $\rho_m = 1890$ ; liquid,  $\rho_l = 1050$ .

$c$  [J/(kg·K)] is the specific heat capacity (at constant pressure).  $c_s = 960$ ;  $c_m = 2610$ ;  $c_l = 4190$ .

$D_{wm}$  [m<sup>2</sup>/s] is the coefficient of binary diffusion of dissolved salt in water.  $D_{wm} = 2 \cdot 10^{-9}$ .

$\lambda$  [W/(m·K)] is the thermal conductivity coefficient.  $\lambda_s = 0.6$ ;  $\lambda_l = 0.8$ . The thermal conductivity of a wet sphere is estimated as

$$\lambda = \epsilon_s \lambda_s + \epsilon_l \lambda_l. \quad (6)$$

$k_{pr}$  [kg/(s·m<sup>3</sup>)] is the precipitation rate constant. The values of  $k_{pr}$  are given in the text.

It is assumed that the liquid density, heat capacity and thermal conductivity are independent on salt concentration. If necessary, these dependencies can be easily taken into account. The main goal of this paper is to demonstrate the model, not to calculate specific examples. Therefore, the parameter values are rather arbitrary.

Variable parameters of the model are the surface tension, the dynamic viscosity and the soluble threshold of salt in water. Formulas for assessing

the physical properties of water vapor and water depending on temperature [°C] are taken from works [7, 8].

Pressure of saturated water vapor  $P_{vp}^*$  [Pa]:

$$P_{vp}^*(T) = 133.32 \exp \left( 18.584 - \frac{3984.2}{233.426 + T} \right). \quad (7)$$

Surface tension of water  $\sigma_w$  [N/m]:

$$\sigma_w(T) = -1.3 \cdot 10^{-7} T^2 - 1.58 \cdot 10^{-4} T + 0.07606. \quad (8)$$

Dynamic viscosity of water  $\mu_w$  [Pa·s]:

$$\mu_w(T) = -1.27 \cdot 10^{-9} T^3 + 3.42 \cdot 10^{-7} T^2 - 3.43 \cdot 10^{-5} T + 1.56 \cdot 10^{-3}. \quad (9)$$

The mass fraction  $\gamma_m^*$  of salt in a saturated solution determines the conditions for precipitation. As an example of the dependence of this parameter on temperature, data on the solubility of ferrous sulfate in water, taken from Wikipedia ([https://en.wikipedia.org/wiki/Iron\(II\)\\_sulfate](https://en.wikipedia.org/wiki/Iron(II)_sulfate)), are used in this work. The dependence of solubility  $S_m^*$  [g per 100ml of water] on temperature in the temperature range of 0-60°C is approximated by the function

$$S_m^*(T) = 0.665T + 14.128, \quad (10)$$

so (assuming the water density is equal 1000 kg/m<sup>3</sup>) the limited mass fraction is defined as

$$\gamma_m^*(T) = \frac{S_m^*(T)}{100 + S_m^*(T)}. \quad (11)$$

The surface tension and viscosity of a solution should depend on the salt concentration. However, information on these relationships is very scarce. Therefore, for the sake of certainty, it is assumed that in a saturated solution

$$\sigma_L^* = k_\sigma \sigma_w, \quad \mu_l^* = k_\mu \mu_w, \quad (12)$$

and a linear dependence in between

$$\sigma_l = \sigma_w + \frac{\gamma_m}{\gamma_m^*} (\sigma_l^* - \sigma_w), \quad \mu_l = \mu_w + \frac{\gamma_m}{\gamma_m^*} (\mu_l^* - \mu_w). \quad (13)$$

In further calculations  $k_\mu = 10$  and  $k_\sigma = 1$ .

### 2.3. Velocity of liquid

The velocity of the liquid  $\mathbf{v}_l$  is determined by Darcy's law

$$\mathbf{v}_l = -\frac{k_l}{\mu_l} \nabla P_l, \quad (14)$$

where  $k_l$  is the permeability of porous material for liquid and  $\mu_l$  is the dynamic viscosity of liquid. The liquid pressure  $P_l$  is defined as

$$P_l = P_g - P_c, \quad (15)$$

where  $P_g$  is the gas pressure in the pores, and  $P_c$  is the capillary pressure of the liquid. Since the gas phase is not taken into account in the model, the gas pressure  $P_g$  is assumed to be constant and equal to the gas pressure  $P_{ex}$  in the drying environment. Therefore, in fact,

$$\mathbf{v}_l = \frac{k_l}{\mu_l} \nabla P_c. \quad (16)$$

The permeability of a porous material is determined by the structure of its pores. In this case, the density function  $dV_p/dr_p$  of the pore volume  $V_p$  distribution by their size (radius)  $r_p$  plays an important role. Like many papers on this topic, we assume that the distribution density has the form of a truncated Gaussian density

$$\frac{dV_p}{dr_p} = \frac{C}{\sigma_p \sqrt{2\pi}} \exp \left[ -\frac{1}{2} \left( \frac{r_p - \bar{r}_p}{\sigma_p} \right)^2 \right], \quad r_p \in (r_{p,1}, r_{p,2}), \quad (17)$$

where  $r_{p,1}$  and  $r_{p,2}$  are the minimum and maximum pore radii,  $\bar{r}_p$  is the average radius, and  $\sigma_p$  is the standard deviation (in a Gaussian distribution).  $C$  is a normalization constant chosen so that the integral of the density over the interval  $(r_{p,1}, r_{p,2})$  (the total pore volume) is equal to the porosity  $\epsilon$ .

To calculate the velocity of a liquid, we use the model of a porous medium as a bundle of capillaries with volume distribution by radius (17). This model assumes that when the medium is soaked, the liquid fills the capillaries in order of increasing radius, and when the liquid dries, it fills them in the reverse order. Thus, the volume occupied by the liquid can be represented as follows:

$$\epsilon_l = \int_{r_{p,1}}^{r_{p,f}} \frac{dV_p}{dr_p} dr_p, \quad (18)$$

where  $r_{p,f}$  is the largest radius of liquid-filled capillaries. For known  $\epsilon_l$ , formula (18) is considered as an equation for unknown  $r_{p,f}$ . By solving this equation, we find  $r_{p,f}(\epsilon_l)$  and calculate the pressure in a capillary with a moving liquid using Young-Laplace formula.

$$P_c(\epsilon_l) = \frac{2\sigma_l \cos(\theta)}{r_{p,f}(\epsilon_l)}, \quad (19)$$

for zero contact angle  $\theta = 0$ . Using the capillary bundle model the permeability of a material to liquid can be estimated as

$$k_l = \frac{1}{8} \int_{r_{p,1}}^{r_{p,f}} r_p^2 \frac{dV_p}{dr_p} dr_p. \quad (20)$$

Formulas (16-20) provide the liquid velocity distribution  $\mathbf{v}_l(r, t)$  for any instant of time  $t$ .

#### 2.4. Boundary and initial conditions

The boundary conditions for system (1)-(4) are specified at the center of the sphere at  $r = 0$  and at the surface at  $r = R$ . At  $r = 0$ , zero fluxes of the system variables are specified. At  $r = R$ , the flow of water is specified in the form of water vapor evaporating from the surface of the sphere:

$$j_v = \epsilon_l(r, t) \beta P_{g,ex} \frac{M_v}{R_g T_{ex}} \ln \left( \frac{P_{g,ex} - P_{v,ex}}{P_{g,ex} - P_v^*(r, t)} \right) \Big|_{r=R}, \quad (21)$$

where  $\beta$  [m/s] is the external mass transfer coefficient ( $\beta = 0.015$  [7]),  $M_v$  ( $= 18$  g/mol) is the molar weight of water vapo,  $R_g$  is the ideal gas constant. The flow of  $\gamma_m$  at  $r = R$  is zero. The heat flow at  $r = R$  consists of two terms: the heat exchange term with the coefficient  $\alpha$  [W/(m<sup>2</sup>·K)] ( $\alpha = 14.25$ ) and the heat transfered by vapr flow  $j_v$

$$j_h = \alpha(T_{ex} - T) + \Delta h_v j_v, \quad (22)$$

where  $\Delta h_v = -2.5 \cdot 10^6$  J/kg is the enthalpy of the vapor.

Initial conditions: the pores are completely filled with a solution with a uniform distribution of the mass fraction of salt and with a uniform distribution of temperature:

$$\epsilon_l(r, 0) = \epsilon, \quad \gamma_m(r, 0) = \gamma_{m,0}, \quad T(r, 0) = T_0. \quad (23)$$

At  $t = 0$  there is no sediment in the pores:

$$\epsilon_m(r, 0) = 0. \quad (24)$$

Note that the state

$$\epsilon_l(r) = 0, \gamma_m(r) = \gamma_m^*(T_{ex}), T(r) = T_{ex}, \quad (25)$$

is a stable stationary state of system (1)-(4) with the specified boundary conditions (21), (22). Due to the uniqueness theorem, the solution with the initial condition (23) will asymptotically approach the stationary state (25) at  $t \rightarrow \infty$ . (Strictly speaking, the solution will never dry completely.) Therefore, we stop solving the problem when the following condition is satisfied

$$\max_r \epsilon_l(r, t) < \delta, \quad (26)$$

for sufficiently small  $\delta$ .

### 2.5. Numerical method

Since most of the terms in equations (1)-(4) have a divergent form, it is natural to use the control volume method for the numerical solution of the system.

The sphere is divided into  $N$  spherical layers by spherical surfaces of radius  $r_k = (k/N)^{1/3}R$ ,  $k = 1, 2, \dots, N$  (the results of calculations with  $N = 100$  are presented below). The volume of each layer equals to  $V/N$ , where  $V$  is the volume of the spherical pellet. The equations (1-4) are integrated over each spherical layer, with the divergent terms being integrated exactly and the mean value theorem being used to estimate the integrals of the non-divergent terms. As a result of integration, a  $4N$  ODE system is obtained, which, after taking into account the boundary conditions, is solved using the MATLAB function 'ode15s'.

## 3. Results

### 3.1. General view

Figure 1 presents a general outline of a particular solution of system (1)-(4). It is assumed that the sphere was impregnated with a salt solution with the mass fraction of salt  $\gamma_{m,0} = 0.2$  at the temperature  $T_0 = 20^\circ\text{C}$  in air at atmospheric pressure  $P_{g,ex} = 101325$  Pa with humidity  $\varphi = 10\%$ . Then the sphere and the surrounding air are quickly heated to a temperature of  $T_{ex} = 40^\circ\text{C}$  and maintained at this temperature until the solution dries, while the gas pressure and the density of water vapor do not change.



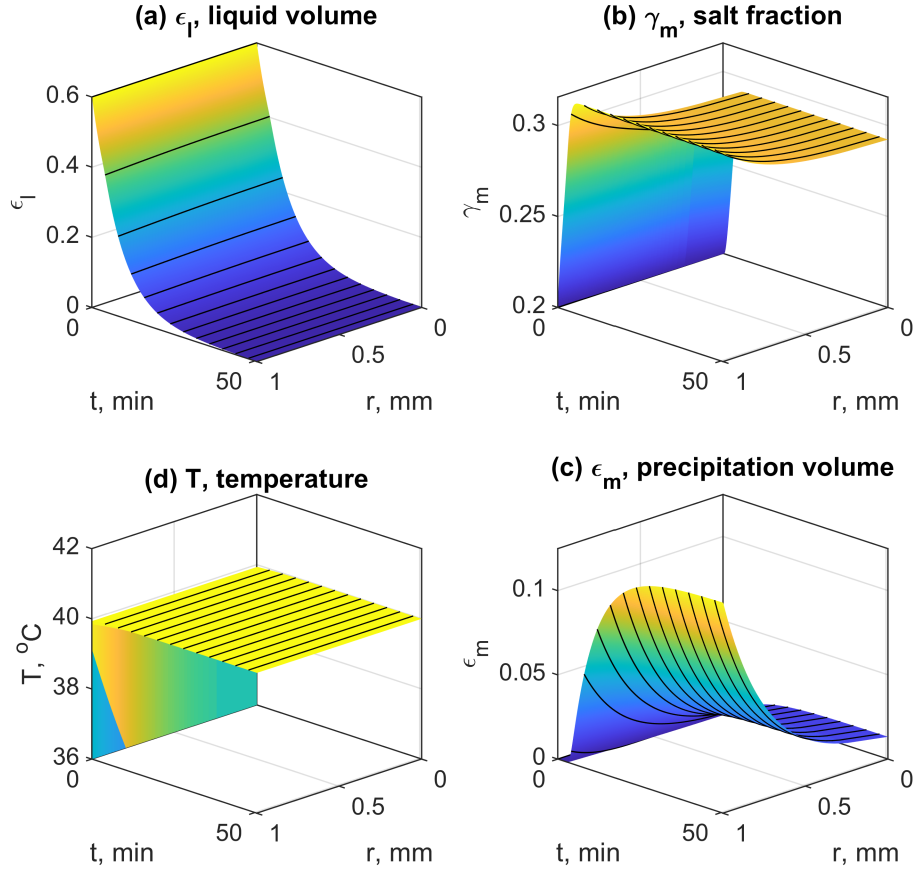


Figure 1: Drying at  $T_{ex} = 40^\circ\text{C}$ . Initial salt mass fraction of salt in solution  $\gamma_{m,0} = 0.2$ . Rate constant of precipitation  $k_{pr} = 50 \text{ kg}/(\text{s}\cdot\text{m}^3)$ . Drying time – 52 min. Lines on the surfaces were drawn at 4-minute intervals.

In subplot (a), the space-time graph of  $\epsilon_l(r, t)$  is shown. At the initial stage of drying (fast stage), for approximately 20 minutes, the volume of the solution in the pores quickly decreases due to the evaporation of water. Then comes the slow drying stage, which lasts for approximately 30 min, until condition (1) with  $\delta = 0.001$  is met. During the slow stage, the reduction in liquid volume occurs mainly due to the precipitation of salt.

The spatiotemporal plot of  $\gamma_m(r, t)$  shown in subplot (b) shows that the salt mass fraction increases rapidly during the fast drying stage and then stabilizes and remains near the saturation value. Salt precipitation is shown in graph (c). It is evident that significantly more precipitation falls in the subsurface layers of the sphere than in the center. The reasons for this phenomenon are discussed in section 3.2. Finally, the temperature in graph (d) remains virtually constant throughout the drying process.

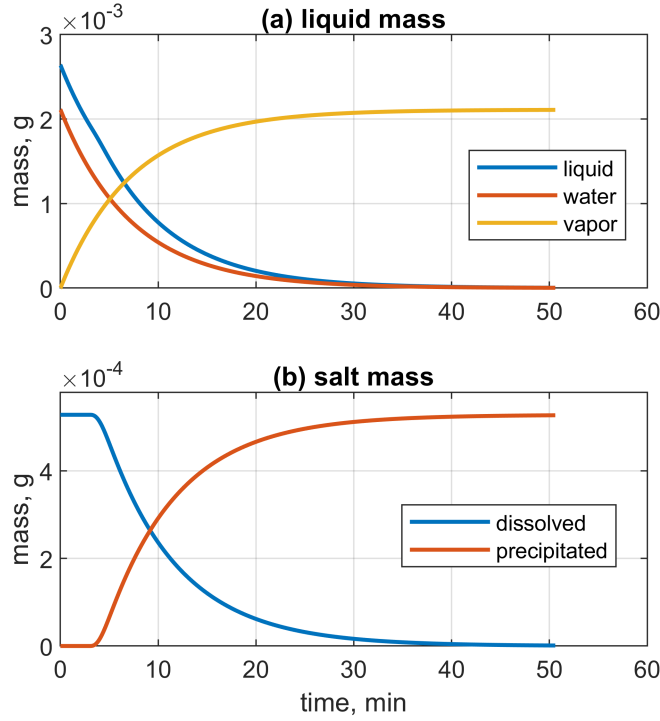


Figure 2: Change in the total mass of substances during drying.

The change in the mass of the substances involved in the process during drying is shown in Figure 2.

### 3.2. Details of precipitation

Figure 3 shows some details of the solution of system (1-4), explaining the features of the process of salt precipitation. Shown here are the graphs relating to the time  $t_* = 15$  min from the solution, the general form of which is shown in Fig. 1.

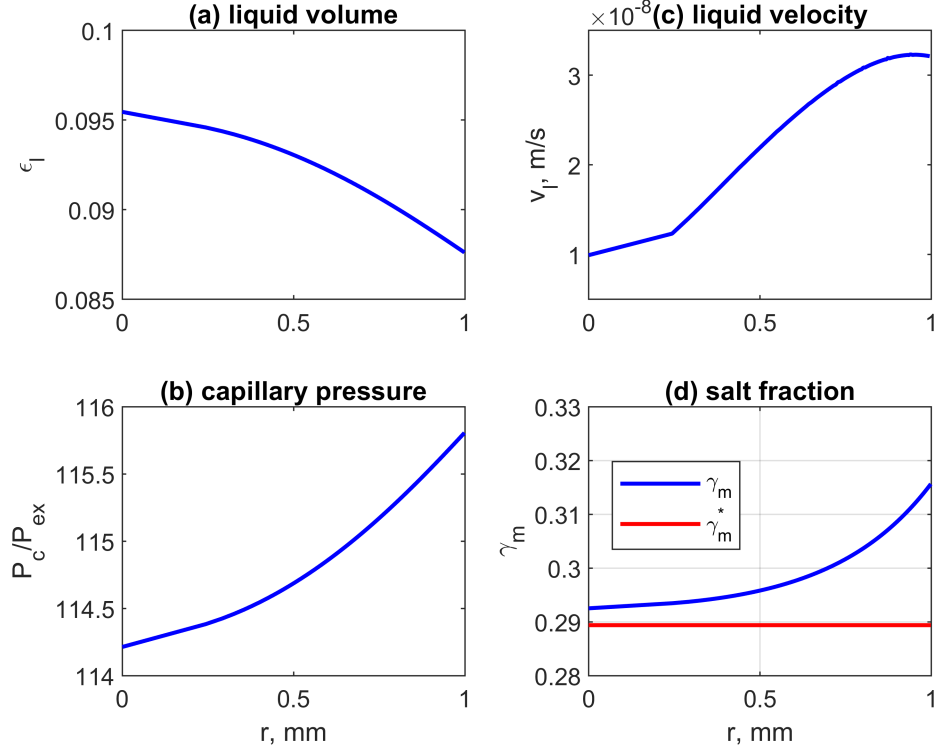


Figure 3: Some details of the solution of system (1-4) at time  $t_* = 15$  min.

From the graph  $\epsilon_l(t_*, r)$ , shown in subplot (a), it follows that the volume occupied by the liquid decreases from the center of the sphere to its periphery. Therefore, the radius  $r_{p,f}$  (eq. (18)) of the largest capillary filled with liquid also decreases and, accordingly, the capillary pressure  $P_c$  (eq. (19)) increases. The graph of capillary pressure  $P_c(t_*, r)$  is shown in subplot (b) in relative units  $P_c/P_{ex}$ , where  $P_{ex}$  is atmospheric pressure.

An increase in the function  $P_c(r)$  leads to a positive liquid velocity  $v_l(r)$ , the graph of which is shown in subplot (c). The liquid flows from the center

to the surface of the sphere, where water evaporates from the solution. The water evaporates, but the salt remains in solution, increasing the salt concentration at the surface of the sphere (subplot (d)). Therefore, the rate of precipitation is greater at the surface of the sphere than at the center.

### 3.3. Distribution of precipitation by radius

A practically important output of the model is the ability to simulate the influence of various factors on the distribution of precipitation along the radius of the sphere after the drying stage.

Figure 4 shows the graphs of the distribution of the salt volume by the radius of the sphere after drying at a temperature of 40°C. The graphs are constructed based on the results of solving the system (1-4) with different initial concentrations of salt in the solution. with increasing mass of salt in the solution, the lines in the figure rise, maintaining their shape.

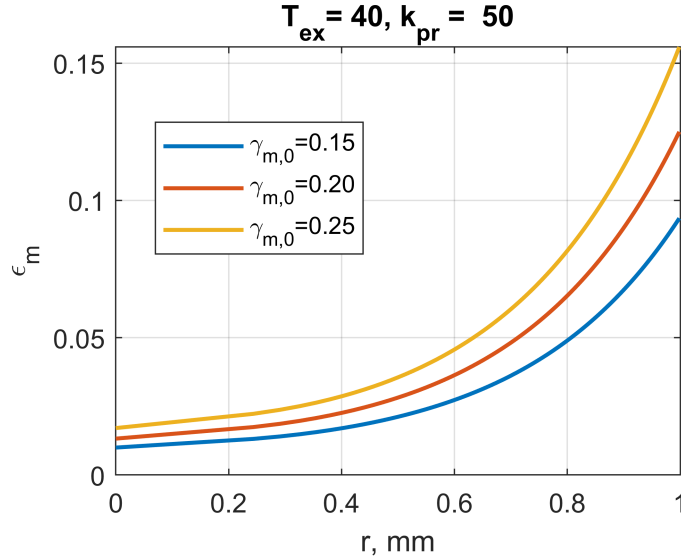


Figure 4: Distribution of precipitations by radius at the end of drying depending on the initial mass fraction of salt.

The following Figure 5 demonstrates the influence of the drying temperature  $T_{ex}$  and the value of the salt precipitation rate constant  $k_{pr}$  on the final distribution of the precipitated salt.

Figure 5a shows that the final salt distribution is virtually independent of drying temperature. Despite the significant differences in drying time: 165

minutes at  $T_{ex} = 20^\circ\text{C}$ , 51 minutes at  $40^\circ\text{C}$ , and 20 minutes at  $60^\circ\text{C}$ , the salt distribution curves are almost identical. Note, however, that at all three temperatures  $T_{ex}$  the value of the constant  $k_{pr}$  was the same and equal to 50.

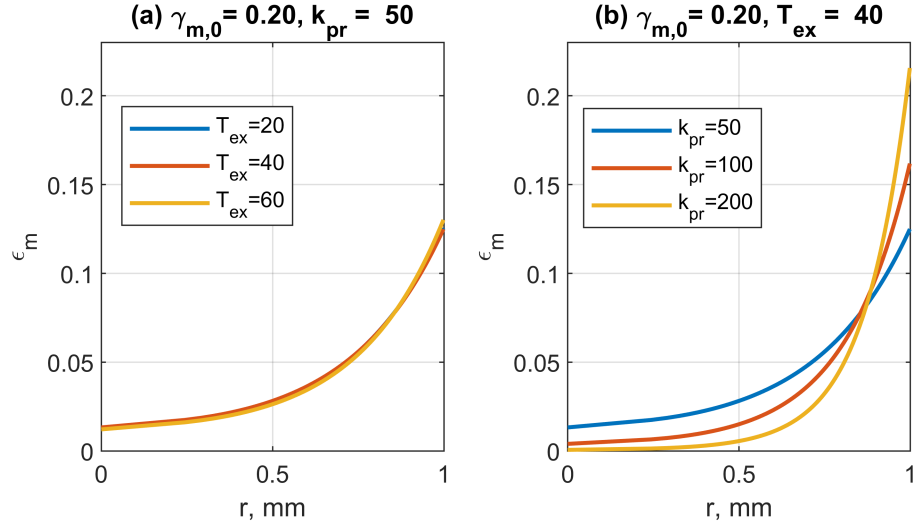


Figure 5: Distribution of precipitation by radius at the end of drying depending on (a) the drying temperature  $t_{ex}$ , (b) the value of constant  $k_{pr}$ .

Figure 5b shows the significant influence of the parameter  $k_{pr}$  on the distribution of precipitated salt after the solution dries. As this constant increases, an increasing volume of salt precipitates in the near-surface region of the sphere and an increasingly smaller volume in its central region. If we assume that the parameter  $k_{pr}$  increases with increasing temperature, then a similar dependence of the distribution on the drying temperature should be observed. As the temperature increases, more and more salt will precipitate near the surface of the sphere.

#### 3.4. Distribution of precipitation by pore size

The capillary bundle model, which is used in the Whitaker model to calculate capillary pressure and liquid velocity, assumes that the liquid in the pores dries in order of decreasing pore size. If we add another assumption to this – namely, that the precipitate precipitates in the pores that are currently drying – then the volume fraction occupied by precipitate distribution by ra-

dus and pore size can be easily calculated. An example of such a distribution is shown in Figure 6.

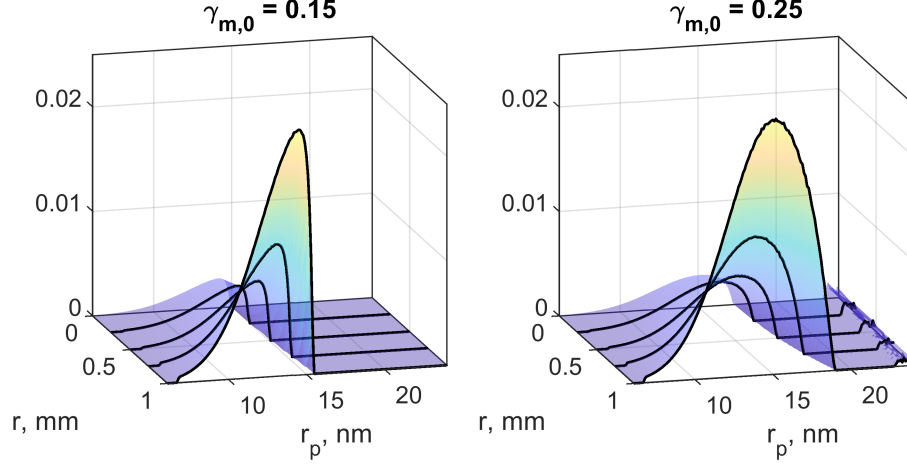


Figure 6: The density of 2D distribution by the radius of the sphere and the pore size of the fraction of the sphere volume occupied by the precipitation after drying at a temperature of  $T_{ex} = 40$  and  $k_{pr} = 50$ . The density is normalized to the total volume of salt,

Salt deposition in pores causes changes in the pore volume distribution by size. These changes are particularly noticeable in the near-surface region of the sphere, where (in the examples discussed here) more salt is deposited. Note that these changes do not affect the results presented above, since the integration in formulas (18), (20) is carried out over capillaries filled with solution, and in them (according to the assumption made) there is no precipitated salt yet, therefore the distribution  $dV_p/dr_p$  at these sizes has not yet changed. However, these changes should be taken into account when simulating re-impregnation of the same pellet with a different solution.

To assess the change in distribution  $dV_p/dr_p$  during drying, one can subtract the distribution of precipitation volume by pore size from the initial distribution. An example of the result of such an operation is shown in Figure 7. This is only an approximate estimate, since it does not take into account the possible change in pore size when sediment falls into them. In addition, during subsequent steps to prepare the catalyst, the salt must turn into a catalytically active substance with a different volume.

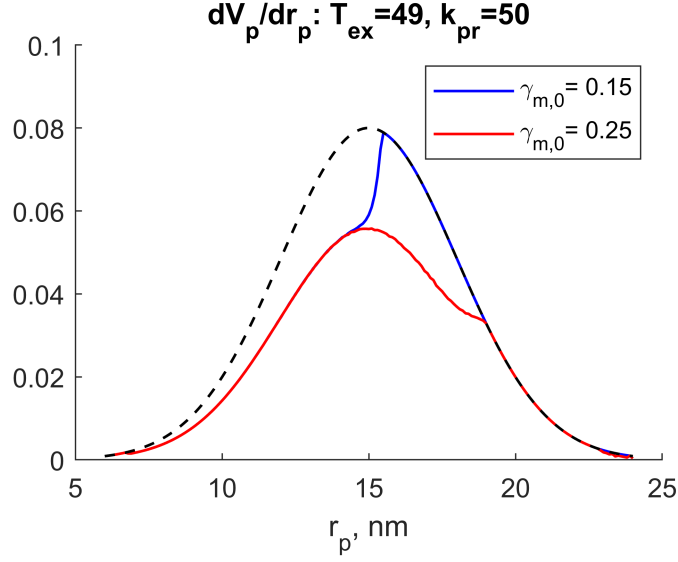


Figure 7: Estimation of the pore volume distribution along the pore size in the near-surface layer of the sphere after drying. In large pores, no precipitate forms because the salt concentration in the solution is less than critical. The dashed line shows the original distribution.,

#### 4. Conclusion

This paper is devoted to mathematical modeling of a complex multiparameter process of forming the spatial distribution of a catalyst precursor in a solution-impregnated porous sphere during the drying stage. The presented model is based on the Whitaker model of drying porous materials (ignoring the gas phase in the pores) and a model of precipitation from a supersaturated solution. The model allows for studying the influence of various factors on the final precipitate distribution. However, only qualitative agreement with experimental data can be expected, since the values of many process parameters are known only approximately. Also, little information is available on the dependence of the physical properties of the solution on temperature and salt concentration.

The drying model uses a representation of the porous medium as a bundle of capillaries of varying sizes. This representation establishes the order of pore drying; the solution in the pores dries in descending order of pore size. Assuming that the precipitate precipitates in the pores that are currently drying, the precipitate distribution by pore size can be estimated. The article

provides an example of calculating the distribution of sediment by the radius of a sphere and the size of pores during drying of a sphere impregnated with a solution of ferrous sulfate.

## Acknowledgments

The author thanks Professor P.A. Chernavskii for helpful discussions.

## References

- [1] Peter Munnik, Petra E. de Jongh, and Krijn P. de Jong. Recent developments in the synthesis of supported catalysts. *Chem. Rev.* **115** (2015) 6687–6718. doi: 10.1021/cr500486u.
- [2] Diksha K. Jambhulkar, Rajendra P. Ugwekar, Bharat A. Bhanvase & Divya P. Barai (2020): A review on solid base heterogeneous catalysts: preparation, characterization and applications, *Chemical Engineering Communications*, doi: 10.1080/00986445.2020.1864623
- [3] RICHARD C. VINCENT AND ROBERT P. MERRILL, Concentration profiles in Impregnation of porous catalysts, *JOURNAL OF CATALYSIS* **35** (1974) 206-217.
- [4] Sheng-Yi Lee and Rutherford Aris The distribution of active ingredients in supported catalysts prepared by Impregnation. *CATAL. REV.-SCI. ENG.*, 27(2) (1985) 207-340. doi: 10.1080/01614948508064737
- [5] Azzeddine Lekhal, Johannes G. Khinast, and Benjamin J. Glasser, Predicting the effect of drying on supported coimpregnation catalysts. *Ind. Eng. Chem. Res.* **40** (2001), 3989-3999. doi: 10.1021/ie010126k
- [6] Xue Liu, Johannes G. Khinast, Benjamin J. Glasser, A parametric investigation of impregnation and drying of supported catalysts. *Chemical Engineering Science* **63** (2008) 4517 – 4530. doi:10.1016/j.ces.2008.06.013
- [7] D.R. Rieder, E.A.J.F. Peters, J.A.M. Kuipers, Modeling the drying process of porous catalysts - impact of viscosity and surface tension. *Chemical Engineering Science* **282** (2023) 119261. doi: 10.1016/j.ces.2023.119261



- [8] David R. Rieder, Elias A. J. F. Peters, and Johannes A. M. Kuipers, Modeling the drying process of porous catalysts: Impact of the pore size distribution. *Ind. Eng. Chem. Res.* **62** (2023) 20006-20016. doi: 10.1021/acs.iecr.3c03057
- [9] Stephen Whitaker, Simultaneous heat, mass, and momentum transfer in porous media: A theory of drying. *Advances in heat transfer*, **13** (1977) 119-203, doi: 10.1016/S0065-2717(08)70223-5
- [10] Hong Thai Vu and Evangelos Tsotsas, A framework and numerical solution of the drying process in porous media by using a continuous model, *International Journal of Chemical Engineering*, Volume 2019, Article ID 9043670, 16 pages, doi: 10.1155/2019/9043670